Available online at www.sciencedirect.com

SciVerse ScienceDirect

Solar Energy 86 (2012) 3288–3300

SOLAR ENERGY

www.elsevier.com/locate/solener

Combined heat and mass transfer analyses in solar distillation systems – The restrictive conditions and a validity range investigation

P.T. Tsilingiris

Department of Energy Engineering, Heat Transfer Laboratory, Technological Education Institution of Athens, A. Spyridonos Street, GR 122 10 Egaleo, Athens, Greece

Received 11 April 2012; received in revised form 30 July 2012; accepted 16 August 2012

Communicated by: Associate Editor G.N. Tiwari

Abstract

The present work aims at the investigation of the validity range and accuracy of earlier developed theories which have been proposed for the modeling of heat and mass transfer within confined spaces in solar distillation systems. The investigation which is based on the evaluation of agreement between theoretical results and an extensive body of earlier field and laboratory measurements covers a very wide range of operating conditions and allows a comparable validation of the earlier proposed theories. It also clearly defines the restrictions, limitations and the validity range in relationship to yield as well as to the operating temperature level, beyond which significant deviations between predictions from both the earlier Dunkle's as well as more recent analogy models and measurements occur for practical solar stills.

Keywords: Solar distillation; Mass transfer; Evaporation heat transfer; Transport processes modeling restrictions

1. Introduction

Seawater desalination is an energy intensive process that is best adapted to the solar energy resources. Solar distillation systems being currently considered as a mature technology may turn out to be vital for the survival of certain island and isolated offshore communities in close to equator arid and semi arid zones. These systems are basically composed of a top glazed cavity containing a saline water layer, which is heated by the transmitted solar radiation through the top glazing cover. This causes water heating, evaporation and transfer of water vapor from the liquid surface through a thin diffusive interface to a uniformly mixed layer of saturated air mixture. The flow of heat and water vapor from this layer through a similar diffusive interface at the top inner glazing surface causes condensation of water vapor, heat rejection and continuous outflow of distillate. When these fundamental processes are carried out once, with the sense that the overall upwards heat flux is directly rejected to the environment, the system can be seen as a single effect unit. When the process is successively repeated in a series of similar single effect units, which recover and reemploy the rejected heat, the systems are usually referred to as multi effect units. In either case, the modeling and prediction of the mass outflow in a typical single effect unit is a matter of a prime importance and depends on the precise evaluation of various complex physical processes, which determine the accuracy of yield prediction of any solar distillation system.

Several decades have passed since Dunkle (1961) first reported results from a complete theoretical analysis on the prediction of combined transport processes within the solar still enclosure of solar distillation systems, which was later discussed in greater detail by Malik et al. (1982). A substantial amount of both theoretical and

E-mail address: ptsiling@teiath.gr

0038-092X/$ - see front matter © 2012 Elsevier Ltd. All rights reserved.
http://dx.doi.org/10.1016/j.solener.2012.08.009

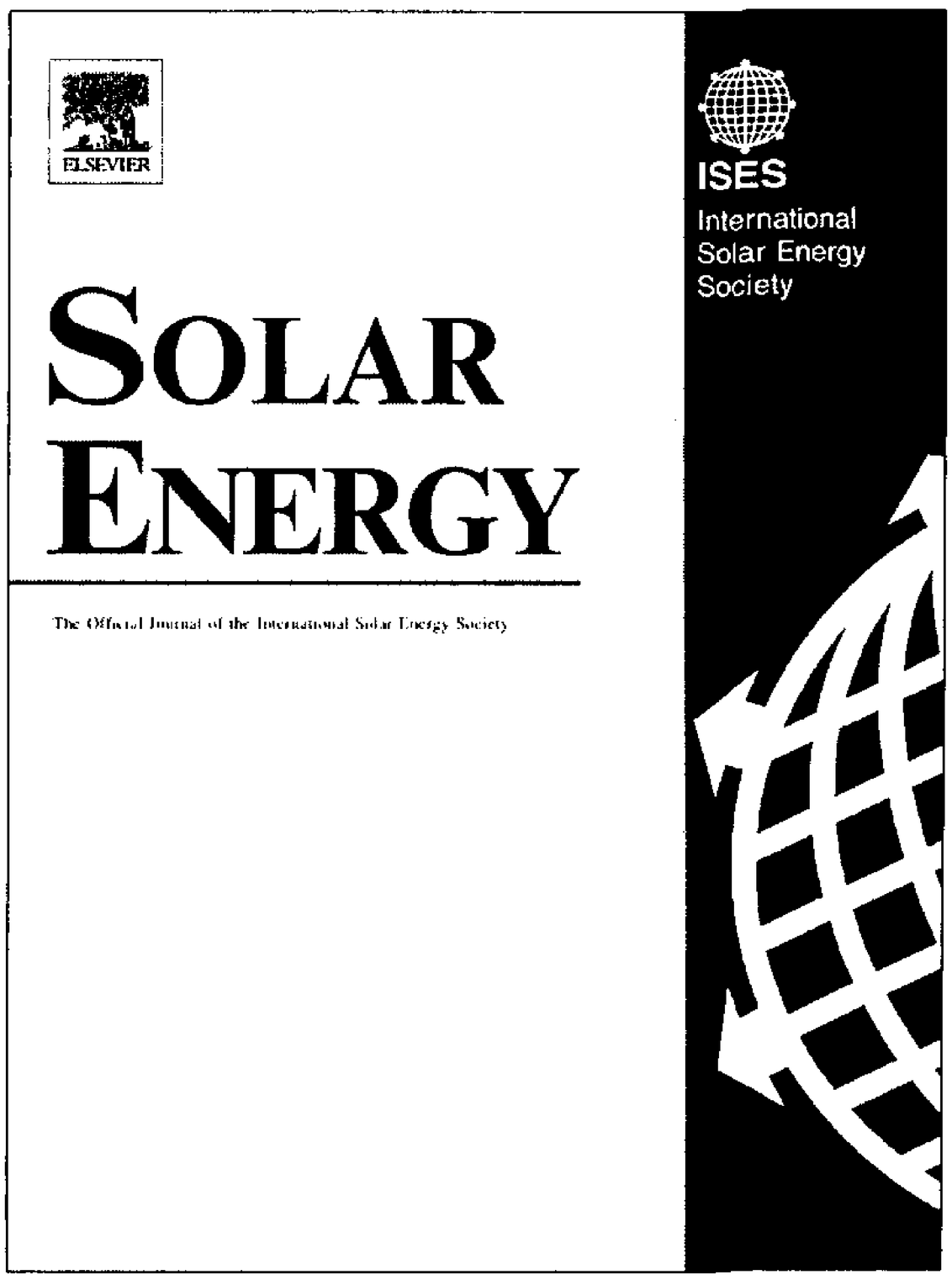

(This is a sample cover image for this issue. The actual cover is not yet available at this time.)

Nomenclature

A_0 to A_4 numerical constants
c_p specific heat capacity (J/kg K)
C numerical constant
C_1 to C_3 numerical constants
D diffusion coefficient (m^2/s)
DA_0 to DA_2 numerical constants
g acceleration gravity (m/s^2)
Gr grashof dimensionless number
h heat (w/m^2 K) or mass (m/s) transfer coefficient
h_{fg} heat of evaporation (kJ/kg)
HF_0 to HF_1 numerical constants
K thermal conductivity (w/m K)
L characteristic length (m)
Le Lewis dimensionless number
$\dot{m}$ per unit still area mass flow rate (kg/m^2 s)
M molar mass (kg/kmol)
n numerical exponent
Nu Nusselt dimensionless number
P pressure (kPa)
Pr Prandtl dimensionless number
R gas constant (kJ/kg K)
Ra Rayleigh dimensionless number
Ra^* modified dimensionless Rayleigh number
t temperature (°C)
T absolute temperature (K)
$\bar{t}$ average temperature (°C), $\bar{t} = \frac{t_w + t_g}{2}$
ΔT temperature difference (°C or K), $\Delta T = T_w - T_g = t_w - t_g$

Greek letters
α thermal diffusivity (m^2/s)
β coefficient of volumetric thermal expansion (K^{-1})
Δ difference
μ viscosity (kg/m s)
ν kinematic viscosity (m^2/s)
ξ dimensional constant (K/Pa)
ρ density (kg/m^3)

Subscripts
a air
cv convective
e evaporative, mass
g glazing
LM logarithmic mean
m mixture, average
ms measured
o total, barometric
p predicted
w water, brine

experimental work has been carried out during the last decades, aiming to acquire a deeper insight on the complex heat and mass transfer processes within the solar still enclosure like those by Kumar and Tiwari (1996), Tiwari et al. (1997), Porta-Gandara et al. (1998, 2004) and to improve the level of confidence on the developed theory as reported by Adhikari et al. (1990), Hongfei et al. (2002), Tiwari et al. (1998) and Tsilingiris (2009, 2011). Except for certain controversial reports that have sporadically appeared in the literature, it is impressive that this theory appears to be successful when it is applied under the appropriate assumptions. Aiming to extend the validity range and improve the prediction accuracy of physical processes, attempts have also been made to develop more universal models mainly based on the heat and mass transfer analogy approach. Shawaqfeh and Farid (1995) have reported an analogy model based on a purposely derived Rayleigh number correlation, which, although it developed overprediction of measurements, was employed for the evaluation of mass transfer in laboratory solar stills. Hongfei et al. (2002) have also developed a theoretical model based on analogy principles, which was properly validated by laboratory measurements at higher temperatures, while Tsilingiris (2010) has recently reported a Chilton–Colburn model which may be proved to be accurate in a broad range of operating conditions and temperatures. The present work aims to define the application restrictions and determine the suitability of the theory originally developed by Dunkle, for predictions in relationship to the wide yield and broad average temperature level range during the operation of solar distillation systems. The investigation also aims to specify the validity range and to underline the limitations of this analysis, to the best of the author's knowledge for the first time at such systematic level, based on extensive experimental evidence mainly relevant to usual operating conditions corresponding to strong turbulence in the solar distillation enclosure. Finally, the present work aims to apply, comparably validate as well as define the accuracy limitations of a Chilton–Colburn analogy model earlier developed by Tsilingiris (2010) for mass transport predictions at a wide range of operating conditions, based on extensive measurements from earlier reports in the literature and more recent field investigations carried out under typical Mediterranean mid summer climatic conditions.

2. The modeling of convective heat transfer in solar distillation systems

The flow of air and water vapor mixture under the effect of a destabilizing temperature gradient in any enclosed

space geometry defined by the liquid and condensing surface at a random orientation is attributed to the natural convection. The investigation of the specific flow conditions and the development of an accurate average Nusselt number correlation is an important engineering problem, the analysis of which basically requires the simultaneous numerical solution of Navier–Stokes, continuity, momentum and energy equations under certain specific boundary and initial conditions and specific simplifying assumptions. A number of theoretical investigations referring to various cavity geometries have been earlier reported in the literature by Djebedjian and Rayan (2000), Corcione (2003), Papanicolaou and Belessiotis (2005), indicating the development of complex velocity fields and flow structures. Additional experimental and flow visualization investigations by Porta-Gandara et al. (1998, 2004), have allowed the recording of vigorous periodic sustained flow processes that give rise to growing vortex flows, which strongly affect the convective heat transfer processes. Aiming at the accurate calculation of the convective heat transfer coefficient in highly inclined solar still enclosures, Kumar and Tiwari (1996), alternatively proposed the application of a procedure for the development of a convective heat transfer correlation specifically derived for the respective cavity, based on a regression analysis.

However, although these procedures may be applied to more complex cavity enclosures, the majority of solar distillation systems refer almost invariably to a very simple geometry, which is basically imposed by the presence of the horizontal liquid and the slightly inclined condensing surfaces.

The convective heat transfer in this simple geometry and the evaluation of the average Nusselt number correlation under the effect of a destabilizing temperature gradient is a classical problem in engineering (Jakob, 1949; McAdams, 1958; Hollands et al., 1975, Hollands, 1984, Tsilingiris, 2011), according to which the following dimensionless parameter correlation has been established in the literature,

$$\mathrm{Nu} = \frac{h_{cv} \cdot L}{k} = C \cdot (\mathrm{Gr} \cdot \mathrm{Pr})^n = C \cdot \mathrm{Ra}^n \tag{1}$$

Regarding the simple horizontal enclosure which is usually the case in low sloping angle glazing surface solar still cavities, it happens that for ordinary destabilizing temperature differentials the convective circulation usually leads to strongly turbulent flow regimes and to appreciably high Rayleigh numbers, mainly attributed to the considerable gap thickness between surfaces. Under these conditions which are relevant to practical solar still operation corresponding to about $\mathrm{Ra} > 10^6$, the numerical constants C and n in (1) are very close to the values of $n = 1/3$ and $C = 0.075$ respectively, for which the convective heat transfer coefficient expression becomes independent of the enclosure geometry.

Dunkle (1961) taking into consideration the correlation (1) and assuming that the driving force for the convective heat transfer is enhanced beyond the level imposed by the temperature differential as occurs in ordinary thermal systems, derived the following expression for the convective heat transfer coefficient,

$$h_{cv} = C_1 \left[t_w - t_g + \frac{[P(t_w) - P(t_g)] \cdot T_w}{C_2 - P(t_w)} \right]^{1/3} \tag{2}$$

This expression with constant dimensional values of $C_1 = 0.884$ and $C_2 = 268.9$, which was derived under the assumption of an average still temperatures around 50 °C and dry air thermophysical properties, has also been proposed by Malik et al. (1982).

According to this and to Tsilingiris (2007) the following expression for the convective heat transfer coefficient has also been proposed,

$$h_{cv} = C \cdot k_m \left(\frac{g \cdot \rho_m \cdot \beta}{\mu_m \cdot \alpha_m} \right)^{1/3} \left[(t_w - t_g) + \frac{T_w \cdot [P(t_w) - P(t_g)] \cdot (M_a - M_w)}{M_a \cdot P_o - P(t_w) \cdot (M_a - M_w)} \right]^{1/3} \tag{3}$$

based on the validity of correlation (1). In an attempt to relax the dry air properties and the restrictive maximum temperature assumptions aiming at a more accurate evaluation of the convective heat transfer coefficient, Tsilingiris (2007, 2008) has developed analyses for the evaluation of the humid air thermophysical properties and specific correlations for the calculation of the corresponding saturation mixture properties as a function of temperature.

For $C = 0.075$ and $\rho_m = 1.04325\ \mathrm{kg/m^3}$, $k_m = 0.0269\ \mathrm{W/m\,K}$, $\mu_m = 1.8641 \times 10^{-5}\ \mathrm{Ns/m^2}$, $\alpha_m = 2.3929 \times 10^{-5}\ \mathrm{m^2/s}$ corresponding to saturated mixture properties at about 50 °C, the expression (3) simplifies to a form identical to (2) with the following values of the dimensional constants, $C_1 = 0.83502$ and $C_2 = 268$ which are about 5.54% and 0.33% lower respectively.

3. The mass transfer coefficient

As it has been demonstrated by Malik et al. (1982) and more recently reported by Tsilingiris (2007), the ratio of the mass to convective heat transfer coefficient in K/Pa is calculated by the expression,

$$\frac{h_e}{h_{cv}} = \frac{h_{fg}}{c_{pa}} \cdot \frac{R_a}{R_w} \cdot \frac{P_o}{[P_o - P(t_w)] \cdot [P_o - P(t_g)]} \tag{4}$$

with P in kPa and h_{fg} and c_{pa} given by the following polynomial fit expressions valid in the temperature range between about 10–100 °C, with constants given in Table 2,

$$P(t) = A_0 + A_1 \cdot t + A_2 \cdot t^2 + A_3 \cdot t^3 + A_4 \cdot t^4 \tag{5}$$

$$h_{fg} = HF_0 + HF_1 \cdot t_w \tag{6}$$

$$c_{pa} = CA_0 + CA_1 \cdot (273 + t) + CA_2 \cdot (273 + t)^2 + CA_3 \cdot (273 + t)^3 + CA_4 \cdot (273 + t)^4 \tag{7}$$

Clearly, an accurate estimation of this ratio depends on initial conditions, operating temperatures, thermophysical properties and h_{fg}, which are parameters that should obviously be specified for the accurate estimate of its value. The expression (4) can be simplified under the assumption of typical operation at up to about 50 °C temperatures when the effect of partial pressures is negligible, $P(t_w) \ll P_o$ and $P(t_g) \ll P_o$ and for fixed values of the involved parameters to the following simple expression,

$$\frac{h_e}{h_{cv}} = \xi \tag{8}$$

Under these conditions the dimensional parameter ξ in (K/Pa) was evaluated by Malik et al. (1982), taking into consideration the appropriate values for the different parameters to the numerical value of 0.0130, although the higher value of 0.01627 was recommended to account for the effect of partial pressures for best representation of the heat and mass transfer phenomena. For negligible partial pressures and 50 °C the numerical value of $\xi = 0.0144$ is derived, which deviates less than about ±10% around the average of the previous values. Since this deviation is comparable or even possibly lower than measurement errors and the uncertainty of numerous influential parameters like the precise enclosure geometry definition, it is believed that this value represents a good first estimate for operation at the specific temperature level.

4. The prediction of distillate mass outflow

It is possible to evaluate the mass outflow of distillate based on ordinary heat and mass balance considerations as reported from Malik et al. (1982). Alternatively it may be possible to apply for this reason procedures based on the analogy approach, similar to those employed by Shawaqfeh and Farid (1995), Hongfei et al. (2002) and Tsilingiris (2010).

4.1. The evaluation of mass outflow based on heat and mass balance approach

Based on simple heat and mass balance considerations the distillate mass outflow in (kg/m^2 s) is calculated as,

$$\dot{m}_w = \frac{h_e \cdot [P(t_w) - P(t_g)]}{h_{fg}(t_w)} \tag{9}$$

Inserting the value of h_{cv} from the expression (2) to (8) and upon substitution in (9) it is derived that,

$$\dot{m}_w = C_3[P(t_w) - P(t_g)] \cdot \left[t_w - t_g + \frac{[P(t_w) - P(t_g)] \cdot (t_w + 273)}{C_2 - P(t_w)}\right]^{1/3} \tag{10}$$

where

$$C_3 = \frac{\xi \cdot C_1}{h_{fg}(t_w)} \tag{11}$$

Based on the original Dunkle's and the more recently reported numerical values of 0.884 and 0.83502 respectively for C_1 and 0.013, 0.0144 and 0.0162 for ξ, the corresponding values for C_3 as shown in Table 1 were estimated, suggesting a typical average value around 5.2×10^{-6}.

Upon substitution of (3) and (4) to (9) it is also derived that,

$$\dot{m}_w = \frac{C \cdot k_m}{c_{pa}} \cdot \frac{R_a}{R_w} \cdot \left(\frac{g \cdot \rho_m \cdot \beta}{\mu_m \cdot \alpha_m}\right)^{1/3} \cdot \left[(t_w - t_g) + \frac{T_w \cdot [P(t_w) - P(t_g)] \cdot (M_a - M_w)}{M_a \cdot P_o - P(t_w) \cdot (M_a - M_w)}\right]^{1/3} \cdot \frac{P_o \cdot [P(t_w) - P(t_g)]}{[P_o - P(t_w)] \cdot [P_o - P(t_g)]} \tag{12}$$

with the saturated mixture thermophysical properties given according to Tsilingiris (2007) by the following polynomial fit expressions,

$$\rho_m = RO_0 + RO_1 \cdot t + RO_2 \cdot t^2 + RO_3 \cdot t^3 \tag{13}$$

$$\mu_m = MU_0 + MU_1 \cdot t + MU_2 \cdot t^2 + MU_3 \cdot t^3 + MU_4 \cdot t^4 \tag{14}$$

$$k_m = K_0 + K_1 \cdot t + K_2 \cdot t^2 + K_3 \cdot t^3 \tag{15}$$

$$\alpha_m = TD_0 + TD_1 \cdot t + TD_2 \cdot t^2 + TD_3 \cdot t^3 \tag{16}$$

valid in the range between 10 and 100 °C with the values of numerical constants as shown in Table 2. Assuming that $P_o \gg P(t_w)$ and $P_o \gg P(t_g)$, something that is valid for operation at medium and lower average operational temperatures and for $C = 0.075$ and thermophysical properties $k_m = 0.0269$ w/m K, $c_{pa} = 1000$ J/kg K, $\rho_m = 1.04325$ kg/m^3, $\mu_m = 1.8641 \times 10^{-5}$ kg/m s, $\alpha_m = 2.3929 \times 10^{-5}$ m^2/s corresponding to about 50 °C, the previous expression becomes,

$$\dot{m}_w = 5.1319 \times 10^{-6} \cdot [P(t_w) - P(t_g)] \cdot \left[t_w - t_g + \frac{[P(t_w) - P(t_g)] \cdot (t_w + 273)}{268 - P(t_w)}\right]^{1/3} \tag{17}$$

Table 1
Typical estimated values of constant C_3 in the expressions (9) and (10).

$C_1 = 0.884$			$C_1 = 0.83502$		
$\xi = 0.0130$	$\xi = 0.0144$	$\xi = 0.0162$	$\xi = 0.0130$	$\xi = 0.0144$	$\xi = 0.0162$
$C_3 = 4.8285 \times 10^{-6}$	$C_3 = 5.3485 \times 10^{-6}$	$C_3 = 6.0171 \times 10^{-6}$	$C_3 = 4.561 \times 10^{-6}$	$C_3 = 5.0522 \times 10^{-6}$	$C_3 = 5.6837 \times 10^{-6}$

Table 2
Values of numerical constants in the fit expressions allowing the evaluation of various thermophysical properties.

Physical quantity	Units	Values of numerical constants and validity range
P Saturated vapor pressure	kPa	$A_0 = 1.131439334$, $A_1 = -3.750393331 \times 10^{-2}$, $A_2 = 5.591559189 \times 10^{-3}$, $A_3 = -6.220459433 \times 10^{-5}$, $A_4 = 1.10581611 \times 10^{-6}$, $10 < t < 100$ °C
h_{fg} Heat of evaporation	kJ/kg	$HF_0 = 2503.94$ and $HF_1 = -2.4515$, $10 < t < 100$ °C
ρ_m Saturated mixture density	kg/m^3	$RO_0 = 1.299995662$, $RO_1 = -6.043625845 \times 10^{-3}$, $RO_2 = 4.697926602 \times 10^{-5}$, $RO_3 = -5.760867827 \times 10^{-7}$, $10 < t < 100$ °C
μ_m Viscosity of saturated mixture	kg/m s	$MU_0 = 1.685731754 \times 10^{-5}$, $MU_1 = 9.151853945 \times 10^{-8}$, $MU_2 = -2.16276222 \times 10^{-9}$, $MU_3 = 3.413922553 \times 10^{-11}$, $MU_4 = -2.644372665 \times 10^{-13}$, $10 < t < 100$ °C
k_m Saturated mixture thermal conductivity	w/m K	$K_0 = 0.02416826077$, $K_1 = 5.526004579 \times 10^{-5}$, $K_2 = 4.631207189 \times 10^{-7}$, $K_3 = -9.489325324 \times 10^{-9}$, $10 < t < 100$ °C
α_m Saturated mixture thermal diffusivity	m^2/s	$TD_0 = 1.881493006 \times 10^{-5}$, $TD_1 = 8.027692454 \times 10^{-8}$, $TD_2 = 1.496456991 \times 10^{-9}$, $TD_3 = -2.112432387 \times 10^{-11}$, $10 < t < 100$ °C
$D_{w,a}$ Diffusion coefficient	m^2/s	$DA_0 = 1.820034881 \times 10^{-5}$, $DA_1 = 1.324098731 \times 10^{-7}$ and $DA_2 = 1.978458093 \times 10^{-10}$, $0 < t < 100$ °C
c_{pa} Specific heat cap. of dry air	kJ/ kg K	$CA_0 = 1.03409$, $CA_1 = -0.284887 \times 10^{-3}$, $CA_2 = 0.7816818 \times 10^{-6}$, $CA_3 = -0.4970786 \times 10^{-9}$ and $CA_4 = 0.1077024 \times 10^{-12}$, $-23 < t < 777$ °C ($250 < T < 1050$ K)
c_{pm} Specific heat cap. of Sat. mixture	kJ/ kg K	$CM_0 = 1.088022802$, $CM_1 = -0.01057758092$, $CM_2 = 4.769110559 \times 10^{-4}$, $CM_3 = -7.898561559 \times 10^{-6}$ and $CM_4 = 5.122303796 \times 10^{-8}$, $10 < t < 100$ °C
Pr Saturated mixture Pr number	(–)	$PR_0 = 0.7215798365$, $PR_1 = -3.703124976 \times 10^{-4}$, $PR_2 = 2.240599044 \times 10^{-5}$, $PR_3 = -4.162785412 \times 10^{-7}$, $PR_4 = 4.969218948 \times 10^{-9}$, $10 < t < 100$ °C

This expression is almost identical to the previously derived (10) with very close numerical values of the dimensional constants $C_3 = 5.1319 \times 10^{-6}$ s m^{-1} K$^{-1/3}$ and $C_2 = 268$ and P in kPa, as compared to $C_3 = 5.2 \times 10^{-6}$ s m^{-1} K$^{-1/3}$ and $C_2 = 268.9$ according to the original analysis by Dunkle.

4.2. The evaluation of mass outflow based on the Chilton–Colburn analogy

Aiming at predictions at a wide range of operational conditions, alternative analyses has been proposed by Tsilingiris (2010) based on the Chilton–Colburn analogy approach which is an extension of the Reynolds analogy. According to this the mass outflow of distillate can be evaluated by the following expression,

$$\frac{\dot{m}_w}{h_{cv}} = \frac{1}{\rho_m \cdot c_{pm}} \cdot \frac{P_a}{P_{LM}} \cdot \frac{1}{R_w} \cdot \left[\frac{P(t_w)}{T_w} - \frac{P(t_g)}{T_g}\right] \cdot \mathrm{Le}^{-2/3} \tag{18}$$

with the convective heat transfer coefficient h_{cv} as derived either from the expressions (2), (3). The specific heat capacity of saturated mixture c_{pm} in the range between 10 and 100 °C is given by the following expression,

$$c_{pm} = CM_0 + CM_1 \cdot t + CM_2 \cdot t^2 + CM_3 \cdot t^3 + CM_4 \cdot t^4 \tag{19}$$

with the numerical values of constants given in Table 2 and P_{LM} which represents the logarithmic mean pressure in Pa given by the following expression,

$$P_{LM} = \frac{[P_a - P(t_w)] - [P_a - P(t_g)]}{\ln \frac{P_a - P(t_w)}{P_a - P(t_g)}} \tag{20}$$

The Lewis number is calculated as,

$$\mathrm{Le} = \frac{\alpha_m}{D(\bar{t})} \tag{21}$$

where D is the diffusion coefficient of water vapor into air. According to a literature review it was found by Tsilingiris (2010) that there is a sufficiently good agreement between results from various earlier reported models, indicating a significant up to 80% increase of its initial value for a corresponding temperature increase between 0 and 100 °C. The numerical results according to the Chapman–Enskog model were taken as typical and were fitted by the following expression

$$D_{w,a}(t) = DA_0 + DA_1 \cdot t + DA_2 \cdot t^2 \tag{22}$$

which is valid at the temperature range $0 < t < 100$ °C with the values of constants given in Table 2. Based on the derived diffusion coefficient from (22) and the thermal diffusivity of saturated vapor mixtures from Tsilingiris (2007), the Lewis number was evaluated from (21) and the mass flow rate was calculated from (18) based on h_{cv} as derived either from (2), (3).

5. Comparative Presentation of Theoretical Predictions and Measurements

A large number of reports from various earlier field as well as laboratory experimental investigations may be employed for the investigation of prediction accuracy and the definition of the validity range of previously developed analyses in a typical single effect distillation unit. This usually comprises of an almost horizontal air gap between a condensing plate at the top and the brine surface at a higher temperature underneath. Among the several selection criteria for the collected earlier measurements was the broad temperature range and diversity of meteorological conditions, the clear definition of the solar still enclosure geometry, as well as the reliability of monitoring system.

5.1. The Description of earlier measurements from the literature

Following previous investigations (Tsilingiris, 2009) a data base of representative earlier measurements from the literature was developed, corresponding to laboratory or field investigations carried out under different meteorological conditions. An extended version of this database will further be referred to as "earlier" measurements for distinction to a massive body of data from a recent investigation (Tsilingiris, 2011) which will further be referred as "recent" measurements. A brief description will first be devoted to the earlier measurements since a more detailed discussion has been previously reported by Tsilingiris (2009).

Referring to these, high temperature laboratory mass transport investigations were carried out by Adhikari et al. (1990), corresponding to a broad range of average temperatures and temperature differences between about 19–84 °C and 12–30 °C respectively, with maximum brine temperatures as high as 92 °C. The measurements by Shawaqfeh and Farid (1995) were carried out in a single slope passive solar still, covering an average solar still temperature range from about 26–60 °C, with typical temperature differences ranging between about 5–9 °C and maximum water temperatures up to about 64 °C. Kumar and Tiwari (1996) presented field measurements from active and passive stills corresponding to average still temperatures ranging between about 38–53 °C, with corresponding temperature differences varying typically from about 4–14 °C respectively with maximum water temperatures up to about 60 °C. Measurements were also carried out by Tiwari et al. (1997) in a carefully controlled laboratory environment using fixed thermostatically controlled brine at 46, 63 and 85 °C and condensing surface temperatures of 28, 56 and 64 °C corresponding to the average still temperature levels of about 28, 55 and 73 °C, with rather unusually high temperature differences of about 36, 17 and 20 °C respectively. Further field investigations covering a broad range of water temperatures up to about 75 °C and average still temperature and temperature differences ranging between about 22–72 °C and 2–12 °C respectively, have also been reported by Aggrawal and Tiwari (1998). Tiwari et al. (1998) have reported a limited number of laboratory measurements corresponding to water temperature of about 43 and 65 °C and as low as 2.4 °C glass temperature using crushed ice for the cooling medium. These cover a range of average temperatures between about 22 and 50 °C with very large temperature differences up to about 62 °C. Aiming to derive convective heat transfer correlations for the specific design of a relatively small enclosure, Hongfei et al. (2002) have carried out measurements corresponding to an average still temperature and a temperature difference ranging between about 37–80 °C, and 6.5–15.5 °C respectively, with a maximum brine temperature as high as 85.5 °C. A substantial body of medium and low temperature field measurements corresponding to average temperatures ranging from about 36 °C down to 7 °C with temperature differences between about 3–15 °C were also derived by Voropoulos et al. (2000) from a large double slope solar still with an unusual cavity geometry with significant dimensions and volume. Although this may be responsible for a completely different correlation than (1) valid with $C = 0.075$ and $n = 1/3$ on which the derivation of (3) and (4) is based on, it was decided to retain indicatively these data for comparisons, although they may represent a lower level of confidence measurements.

Almost all previous measurements have been carried out in simple slightly sloped trapezoid or low inclination V shaped geometry enclosures, which very slightly deviates from the parallel plate geometry with a typically 0.15 m gap and vertical adiabatic walls. They also correspond to appreciably high modified Rayleigh numbers, typically $Ra^* \geqslant 10^6$, except of few measurements like those by Aggrawal and Tiwari which may also include data of slightly lower values. These operating conditions for the given simple solar still geometry enclosure being relevant to strong turbulence, recommends the validity of the expressions (2) and (3) for the convective heat transfer coefficient.

5.2. The description of recent field measurements

Additional field measurements have been also recently reported by Tsilingiris (2011), which were carried out during several daily runs using a shallow, passive, carefully insulated, single sloped trapezoidal cavity of simple geometry and low heat capacity, with a glazing inclination of about 15° under typical hot and dry meteorological conditions corresponding to a mid summer Mediterranean climate.

Although brine temperatures as high as 75 °C were recorded, which is believed that represent on average the highest typically obtainable temperature using passive solar distillers of ordinary design under the specified weather conditions, the calculated maximum recorded average still temperature scarcely exceeded 70 °C, with temperature differences typically between 5 and 10 °C.

Under these conditions, although the measured yields were found to vary within a comparatively narrow range between about 0.003–0.2 gr/m^2 s, a small fraction of these data, typically less than about 5% of the sample, correspond to $Ra^* \leqslant 10^6$. These limited measurements representing very low yields, were ignored as being of a lower accuracy and reliability owing to the respective lower Ra^* numbers for which the correlation (1) with $C = 0.075$ and $n = 1/3$, valid for conditions of strong turbulence may not be valid with a sufficient accuracy, as well as due to the degraded mass measurement accuracy level at very low yields.

5.3. The temperature level of measurements

The distribution of the average temperature and temperature difference in the available sample of measurements is

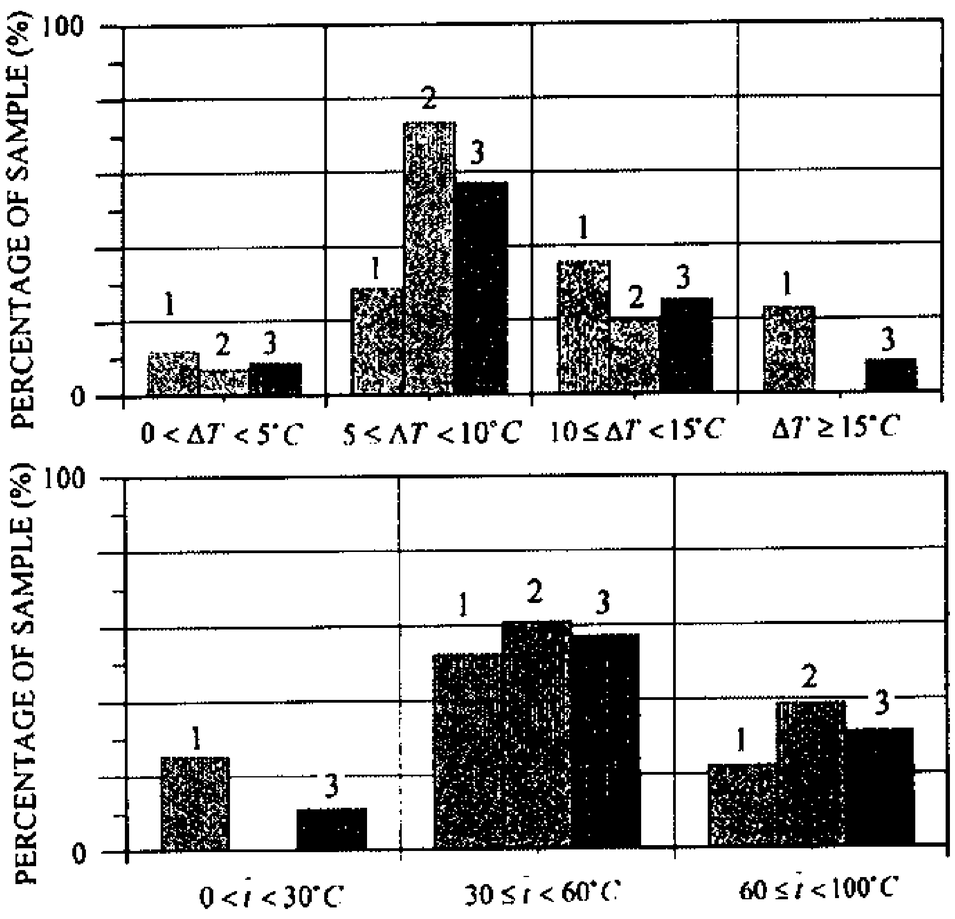

Fig. 1. Temperature difference and average temperature data statistics are shown, with bars 1, 2 and 3 corresponding to the earlier, recent and total set of measurements.

shown in Fig. 1, in which bars (1)–(3) correspond to the earlier and recent subsets as well as the complete set of data respectively. It is indicated that the highest fraction of the complete set of data corresponds to relatively high ΔT, since about 58% and 26% belong to the regions of $5 \leqslant \Delta T < 10$ °C and $10 \leqslant \Delta T < 15$ °C respectively, while the 36% and more than 23% of the earlier reported measurements belong to high and very high ranges of $10 \leqslant \Delta T < 15$ °C and $\Delta T \geqslant 15$ °C respectively. In contrast, almost 74% of the recent measurements correspond to the range of ΔT between $5 \leqslant \Delta T < 10$ °C, while there is a complete lack of data for very high $\Delta T > 15$ °C. These fractions shift the average ΔT of the sample close to a mean value around 10 °C, over which more than 82% of the data distributes.

Regarding the respective distribution of average temperature, it is shown that almost about 57% of data correspond to the intermediate temperature range of $30 \leq \bar{t} < 60$ °C, while more than about 31% and 11% belongs to the high and low temperature regions of $\bar{t} \geq 60$ °C and $\bar{t} < 30$ °C respectively, which identifies the complete sample as medium to higher temperature measurements. Referring to the earlier reported measurements, although fractions of about 23% and 26% belongs to high $60 \leq \bar{t} < 100$ °C, and low $0 \leq \bar{t} < 30$ °C average temperature regions respectively with maximum up to about 83 °C, more than 50% correspond to the range between $30 \leq \bar{t} < 60$ °C, with the sample being spread over an appreciably wide average temperature range. As far as the recent measurements are concerned, it can be seen that although data at the low temperature range are completely lacking, more than about 60% and almost 40% correspond to the $30 \leq \bar{t} < 60$ °C and $\bar{t} \geq 60$ °C regions respectively, although covering a relatively narrow range between about 40 and 65 °C with a comparably lower maximum average temperature of about 72 °C.

6. Results and discussion

Aiming to validate the prediction accuracy of the previously presented theory, the earlier measurements from the literature were first compared with predictions from the fundamental Dunkle's model. Towards this aim, for each pair of the measured t_w and t_g the h_{cv} was calculated from (2) and the h_e and $\dot{m}_w$ were evaluated from expressions (8) for $\xi = 0.0162$ and (10) for $C_3 = 6.017 \times 10^{-6}$. The derived results were plotted in Fig. 2 which indicates a fairly good agreement between predictions and measurements, at least as far as yields between about 0.008 and 0.3 gr/m^2 s is concerned, with a tendency towards underprediction at higher yields. Aiming to quantify the degree of agreement in respect to the yield, all data were classified into two operating level groups corresponding to the lower, $\dot{m}_w < 0.1$ gr/m^2 s and the higher $\dot{m}_w \geqslant 0.1$ gr/m^2 s range of yields respectively. The following linear fit expressions were developed and plotted with broken lines in the same figure,

$$\dot{m}_{w,p} = 1.12042 \cdot \dot{m}_{w,ms} - 0.00294 \qquad \text{COD} = 0.7718 \qquad (23)$$

$$\dot{m}_{w,p} = 0.58971 \cdot \dot{m}_{w,ms} + 0.12266 \qquad \text{COD} = 0.8353 \qquad (24)$$

corresponding to both groups with the respective coefficients of determination (COD). The expression (23) confirms a fairly good agreement between predictions and measurements for the range of the lower yields although the expression (24) demonstrates a degraded accuracy for higher yields, as it is indicated by the growing deviation of fit expression (24) from the unity slope line for

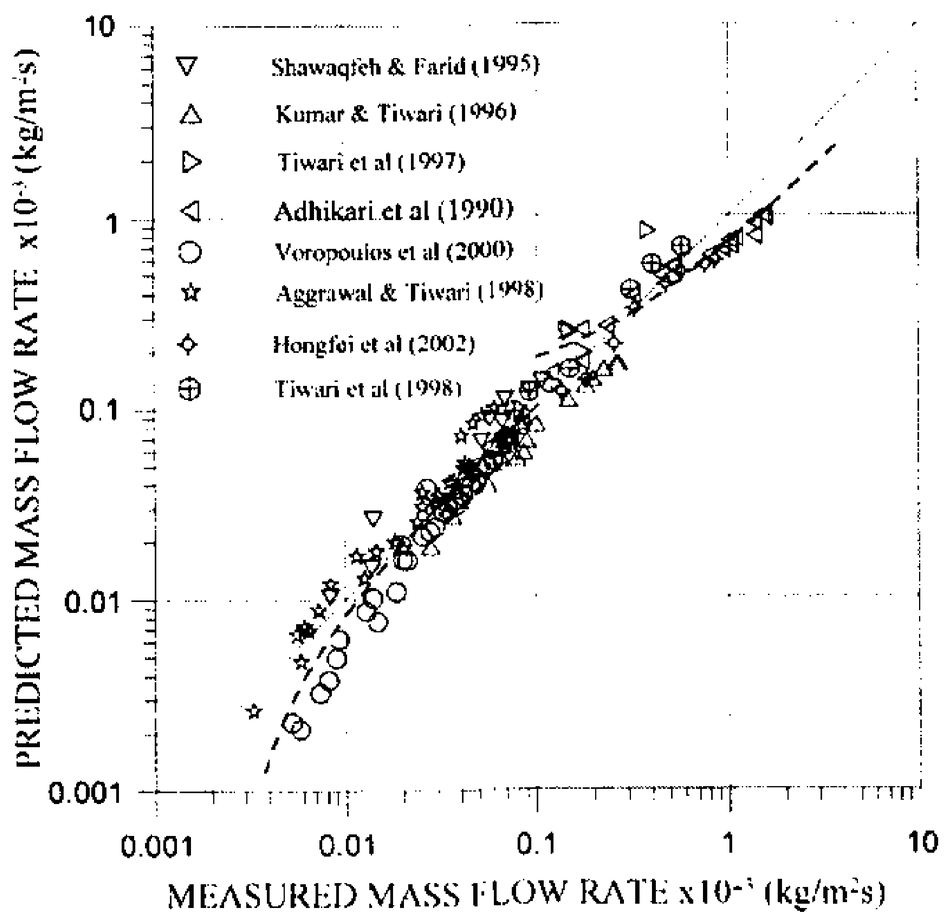

Fig. 2. The yield measurements plotted against predictions according to simple Dunkle's model for the subset of earlier data.

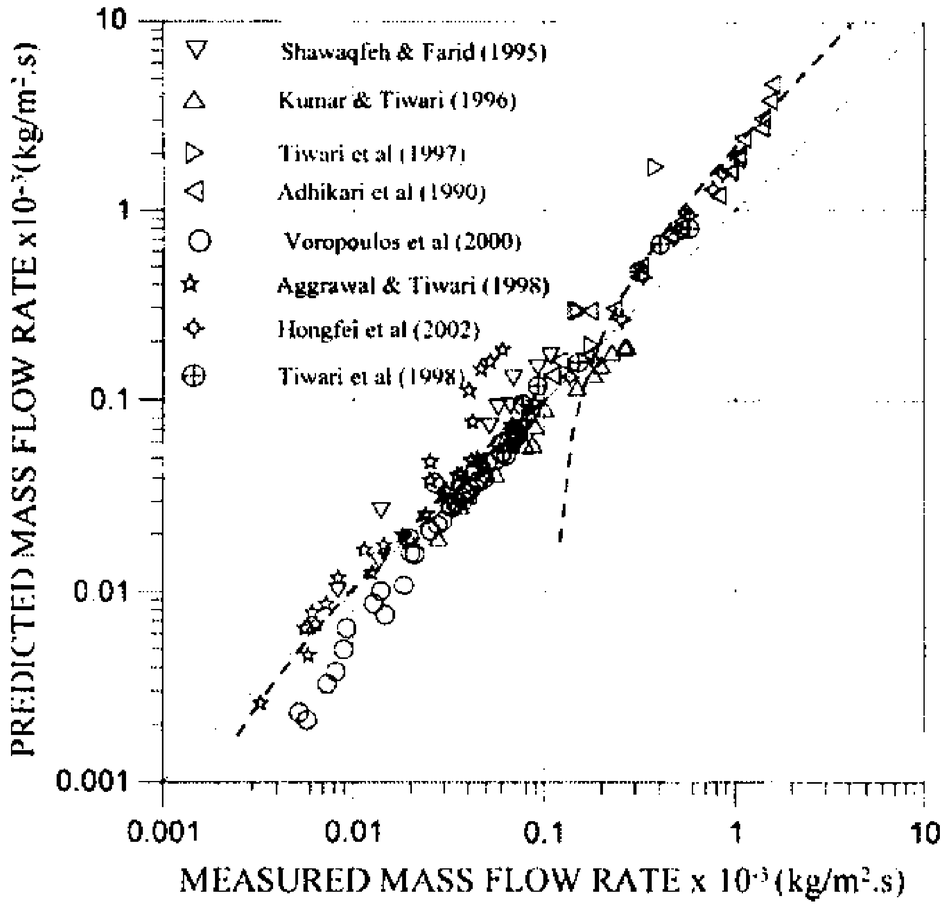

Fig. 3. The yield measurements plotted against predictions according to results from the refined Dunkle's model for the subset of earlier data.

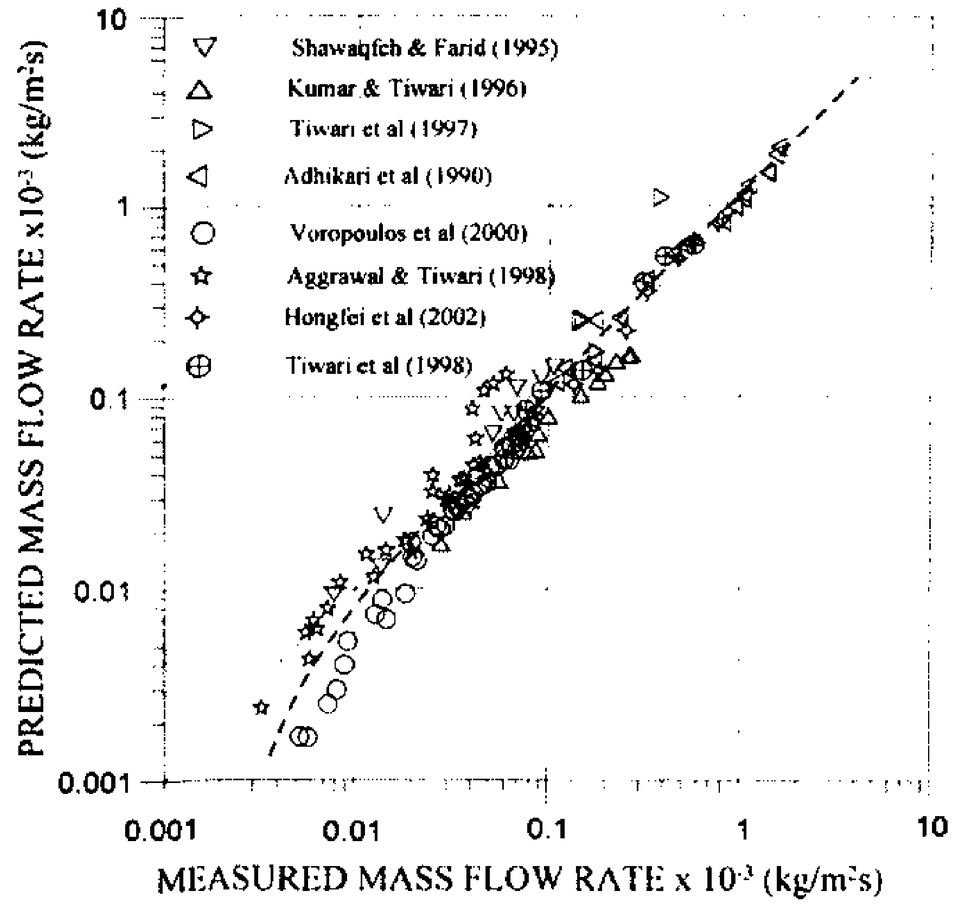

Fig. 4. The yield measurements plotted against predictions according to results from the Chilton–Colburn model and h_{cv} from the basic expression (2) for the subset of earlier data.

$\dot{m}_{w,ms} \geq 0.3$ gr/m^2 s, something that has been also previously noticed by Adhikari et al. (1990) and Clark (1990).

Aiming to validate the prediction accuracy of the refined Dunkle's model, h_{cv} was calculated from (3) and employed for the evaluation of yield from expressions (4) and (12), taking into consideration the saturated mixture thermophysical properties, with the results plotted in Fig. 3. For the previously defined two yield ranges the following linear fit expressions were derived and plotted in the same figure,

$$\dot{m}_{w,p} = 1.15164 \cdot \dot{m}_{w,ms} - 0.00113 \qquad \text{COD} = 0.6079 \qquad (25)$$

$$\dot{m}_{w,p} = 2.45125 \cdot \dot{m}_{w,ms} - 0.27500 \qquad \text{COD} = 0.9173 \qquad (26)$$

These confirm a fairly good agreement between predictions and measurements at the lower range of yields, although they indicate a growing overprediction at higher than about 0.2 gr/m^2 s yields as it is shown by the shift of the corresponding linear fit line (26) to higher slopes.

For the purpose of evaluating the prediction accuracy of the Chilton–Colburn analogy model, the Lewis number was evaluated from (21) based on the α_m values from (16) and $D_{w,a}$ from (22). The mass outflow was then calculated from (18) based on the evaluation of h_{cv} from either the expressions (2), (3). Following the previous calculations based on the evaluation of the h_{cv} from the simplified expression (2), the results were plotted in Fig. 4, showing a very good agreement between predictions and measurements in the whole range of yields. This is confirmed by the following fit expressions plotted in the same figure for the two groups of low and high mass flow rates respectively,

$$\dot{m}_{w,p} = 1.05583 \cdot \dot{m}_{w,ms} - 0.00255 \qquad \text{COD} = 0.6855 \qquad (27)$$

$$\dot{m}_{w,p} = 1.18044 \cdot \dot{m}_{w,ms} - 0.01240 \qquad \text{COD} = 0.9355 \qquad (28)$$

Comparative calculations from the same model although based on the more accurate expression (3) were carried out with the results plotted in Fig. 5. An excellent agreement between results is derived from the whole range of yields, something which is confirmed by the following linear fit expressions, which were plotted in the same figure with broken lines.

$$\dot{m}_{p} = 0.96026 \cdot \dot{m}_{ms} - 0.00070 \qquad \text{COD} = 0.7448 \qquad (29)$$

$$\dot{m}_{p} = 1.01352 \cdot \dot{m}_{ms} - 0.01039 \qquad \text{COD} = 0.9328 \qquad (30)$$

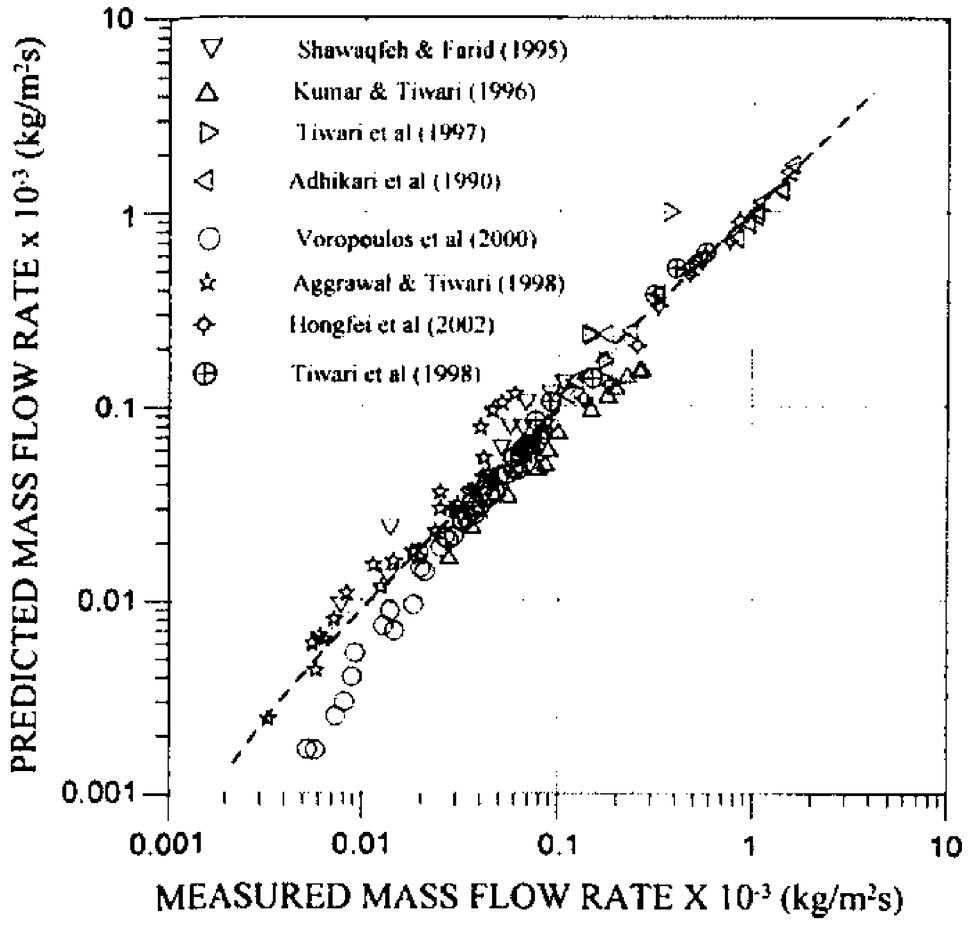

Fig. 5. The yield measurements plotted against predictions according to results from the Chilton–Colburn model and h_{cv} from the refined expression (3) for the subset of earlier data.

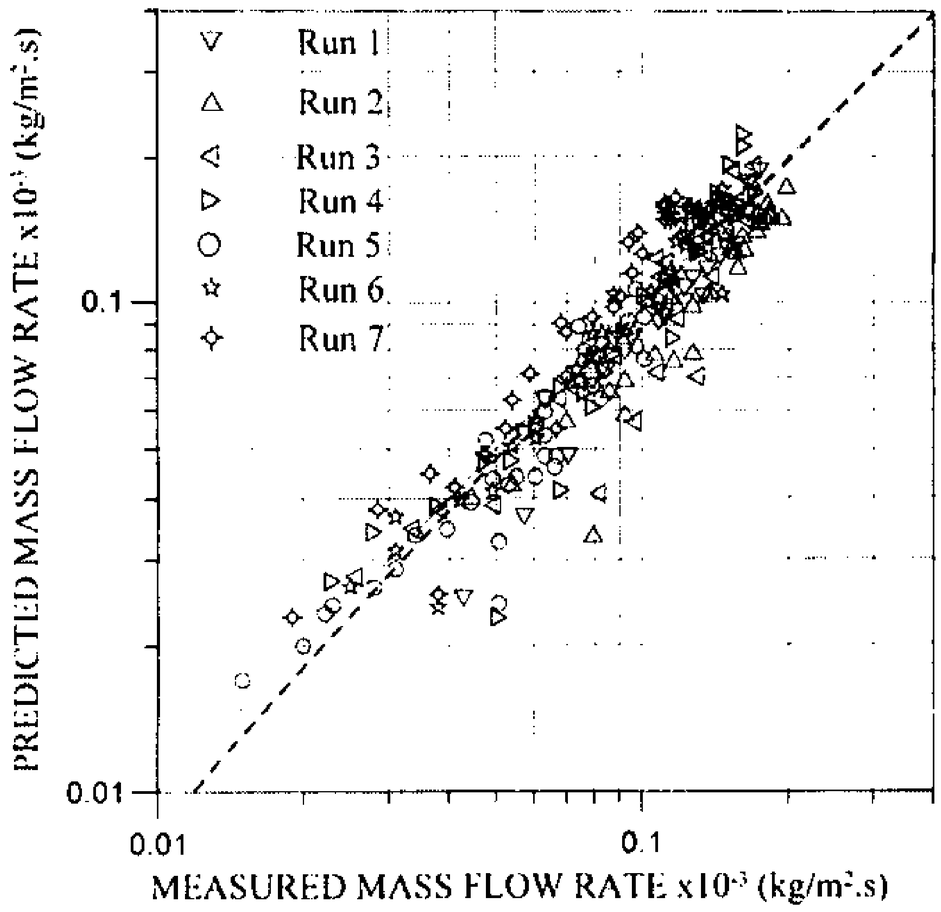

Fig. 6. The yield measurements plotted against predictions according to simple Dunkle's model for the subset of the recent data.

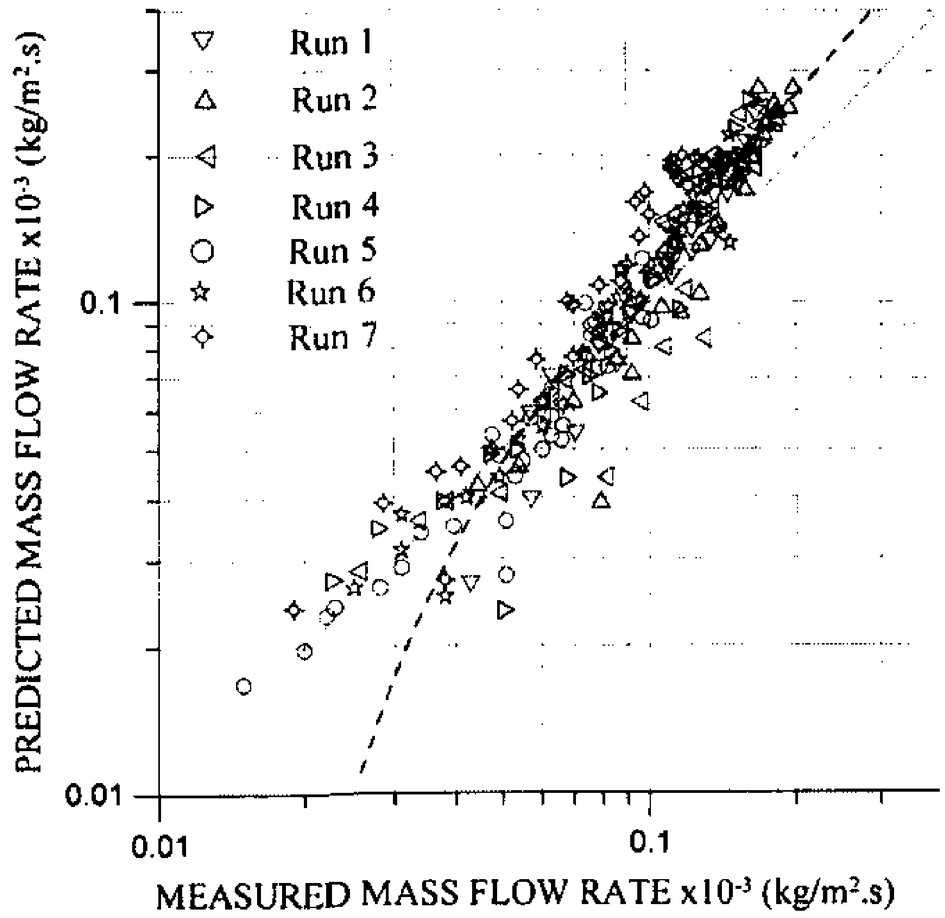

Fig. 7. The yield measurements plotted against predictions according to results from the refined Dunkle's model for the subset of recent data.

Similar calculations of theoretical predictions were also carried out for the recently reported experimental data from the passive solar stills. The comparative results as derived according to the fundamental Dunkle's model expression (2) were plotted in Fig. 6. These were fitted by the following fit expression,

$$\dot{m}_{w,p} = 0.98972 \cdot \dot{m}_{w,ms} - 0.00179 \qquad \mathrm{COD} = 0.8302 \qquad (31)$$

which was plotted in the same figure and confirms a very close agreement between predictions and measurements, at least as far as the entire range of measured yield between about 0.02 and 0.2 gr/m^2 s is concerned.

Respective results derived from the refined Dunkle's model, based on the calculation of the convective heat transfer coefficient from (3) which was employed for the evaluation of yield from (12), were comparatively plotted with measurements in Fig. 7. It is shown that although at lower yields there is a good agreement between results, the model tends to overpredict measurements at higher than about 0.1 gr/m^2 s yields, as confirmed by the following fit expression plotted in broken line,

$$\dot{m}_{w,p} = 1.47589 \cdot \dot{m}_{w,ms} - 0.02692 \qquad \mathrm{COD} = 0.8956 \qquad (32)$$

indicating a substantial deviation from the unity slope line.

Comparative results as derived from the application of the Chilton–Colburn analogy model based on the simplified convective heat transfer coefficient expression (2) are presented in Fig. 8, which shows a close agreement between predictions and measurements as confirmed by the following plotted best fit broken line,

$$\dot{m}_{w,p} = 1.15088 \cdot \dot{m}_{w,ms} - 0.01424 \qquad \mathrm{COD} = 0.8448 \qquad (33)$$

Aiming to validate the capability of a single model to allow accurate predictions in the entire range of yields covering more than three orders of magnitude, the complete

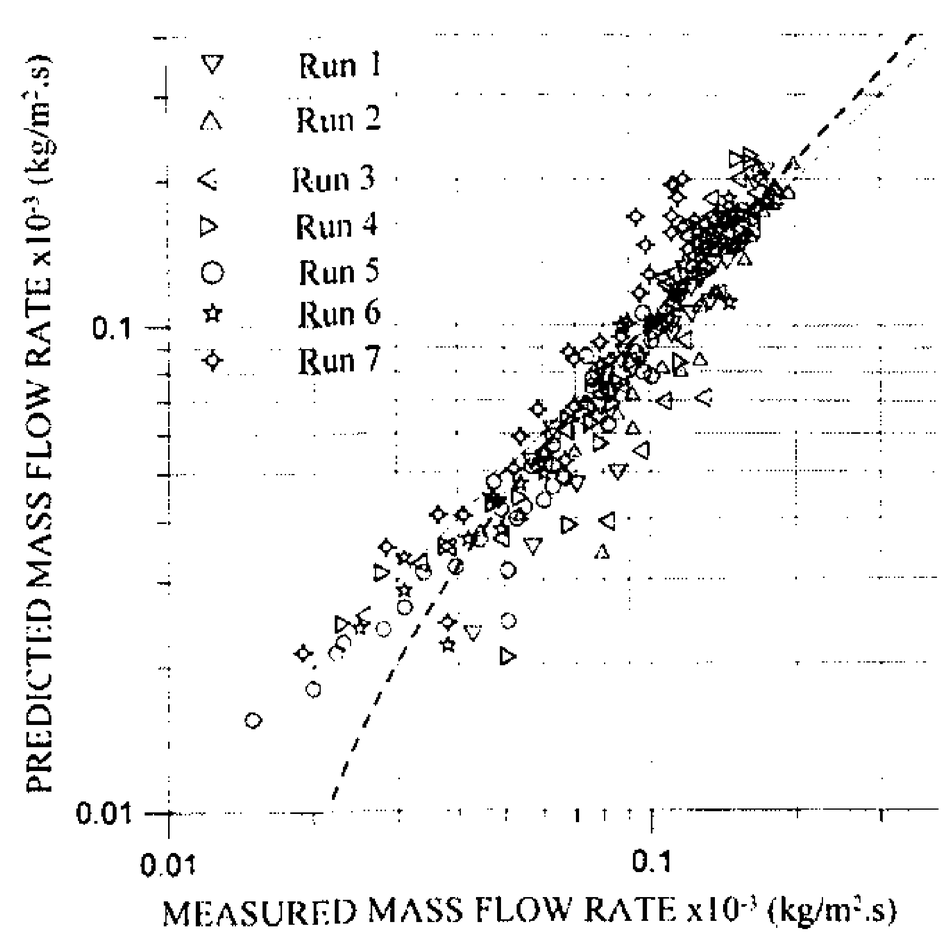

Fig. 8. The yield measurements plotted against predictions according to results from the Chilton–Colburn model and h_{cv} from the basic expression (2) for the subset of recent data.

set of available data was plotted against predictions according to the simplified Dunkle's model in Fig. 9 with uniform data points. These scatter close to the unity slope line suggesting a very good agreement between predictions and measurements up to about 0.5 gr/m^2 s. However this is not valid at higher yields as it has also been earlier noticed by Adhikari et al. (1990), Clark (1990) and Tsilingiris (2009), where the model appears to fail leading to underprediction of measurements, although practical field operation corresponding to higher than about 0.2 gr/m^2 s

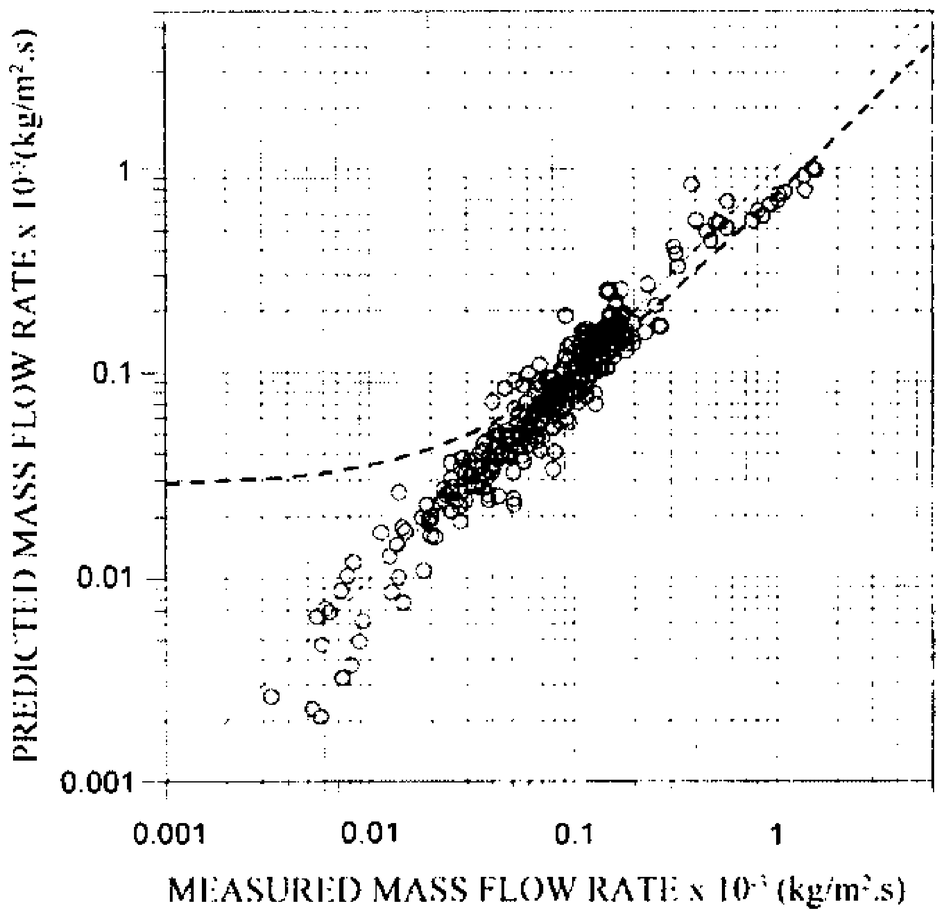

Fig. 9. The yield measurements plotted against predictions according to results from the basic Dunkle's model for the complete set of earlier and more recent data.

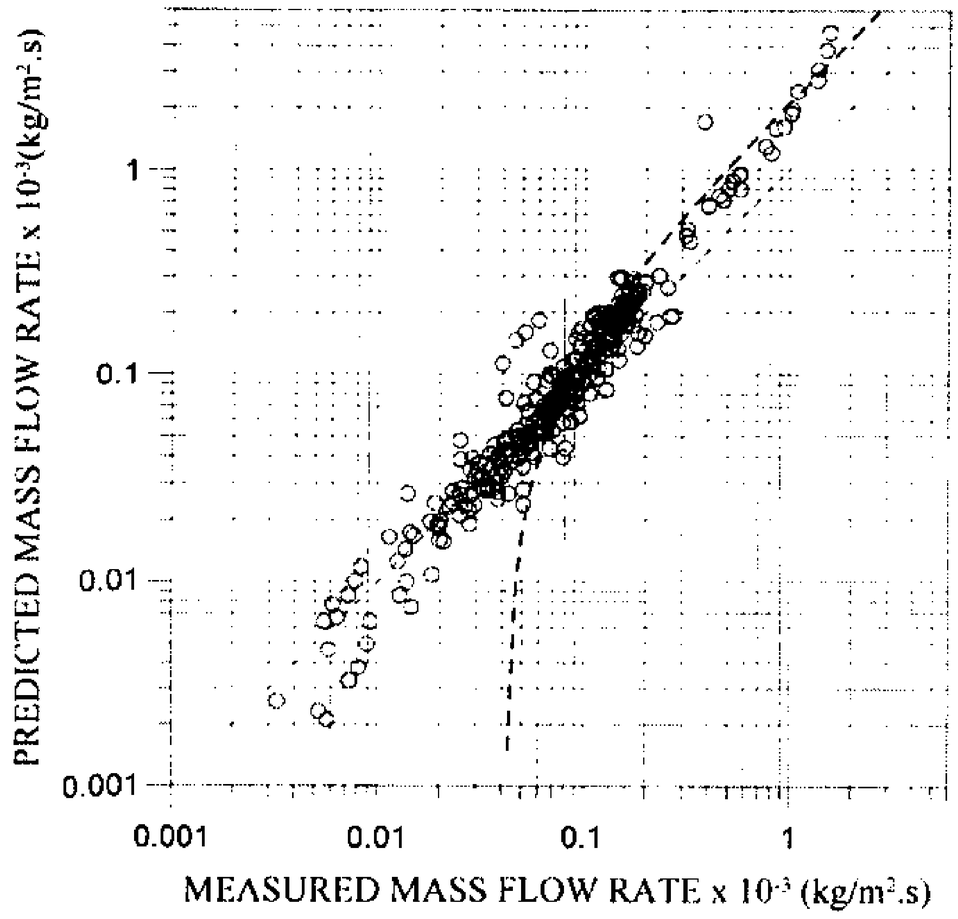

Fig. 10. The yield measurements plotted against predictions according to results from the refined Dunkle's model for the complete set of earlier and more recent data.

yields may be scarce and rather unusual for passive solar stills of ordinary design, even under favorable meteorological conditions.

Aiming to demonstrate the prediction accuracy of this model in the whole range of yields the following linear fit expression was developed,

$$\dot{m}_{w,p} = 0.70659 \cdot \dot{m}_{w,ms} + 0.02822 \qquad \mathrm{COD} = 0.8914 \qquad (34)$$

which indicates that owing to the inefficiency of the model, the plotted best fit line shifts to appreciably lower than the unity slope line at higher than about 0.6 gr/m^2 s yields, confirming the incapability for accurate predictions in the whole range of yields between 0.001 and 6 gr/m^2 s.

The corresponding results from the refined Dunkle's model are shown in Fig. 10, which indicates a growing overprediction of yield as it is demonstrated by the following linear fit expression,

$$\dot{m}_{w,p} = 2.21184 \cdot \dot{m}_{w,ms} - 0.09365 \qquad \mathrm{COD} = 0.9276 \qquad (35)$$

This develops an appreciably higher than unity slope owing to the overprediction for higher than about 0.1 gr/m^2 s yields, something which also suggests the inefficiency of this model for accurate predictions in the entire range of yields.

Comparative results from the Chilton–Colburn analogy model using the approximate convective heat transfer coefficient expression (2), were comparatively plotted against measurements in the Fig. 11. A substantial improvement of the prediction accuracy is demonstrated by the close distribution of data within the unity slope diagonal line as it is indicated by the following plotted linear fit expression,

$$\dot{m}_{w,p} = 1.17833 \cdot \dot{m}_{w,ms} - 0.01392 \qquad \mathrm{COD} = 0.9577 \qquad (36)$$

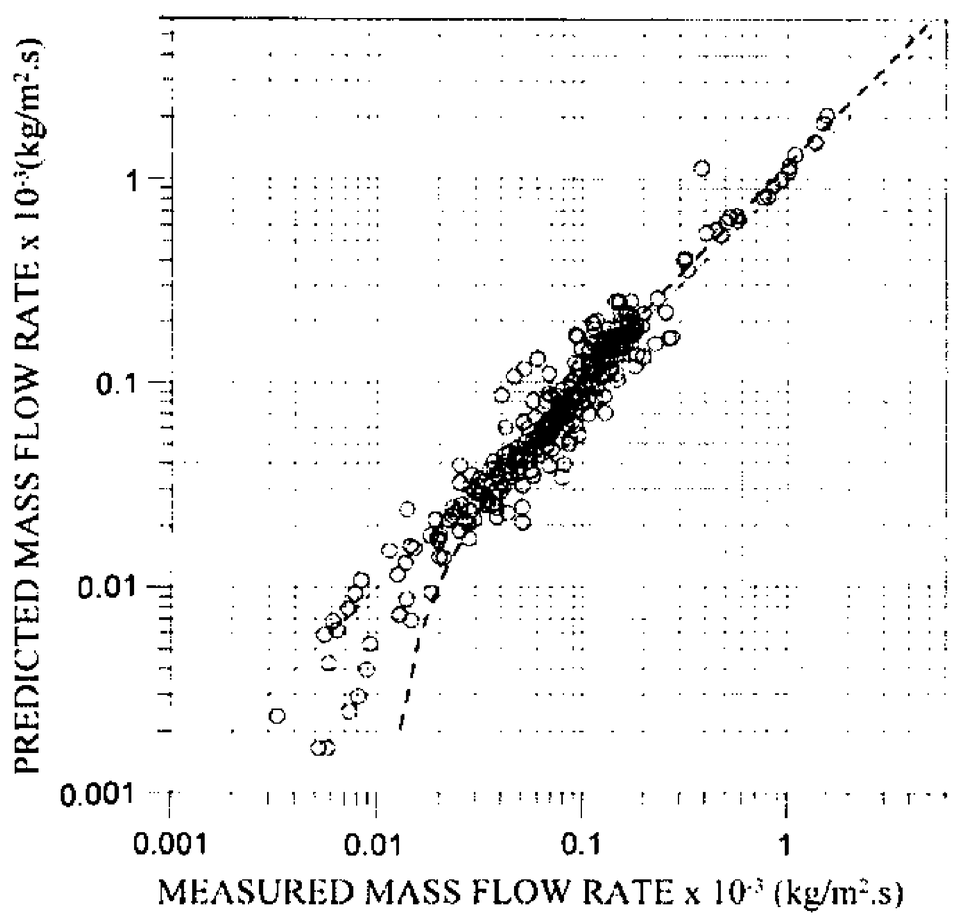

Fig. 11. The yield measurements plotted against predictions according to results from the Chilton–Colburn model and h_{cv} from the basic expression (2) for the complete set of earlier and more recent data.

which suggests a fairly accurate prediction of measurements almost in the entire range of operating temperatures and yields up to about 2 gr/m^2 s.

Corresponding results according to the same model using the more accurate expression (3) were comparatively plotted against measurements in Fig. 12. An excellent agreement is developed which is confirmed by the following plotted linear fit expression,

$$\dot{m}_{w,p} = 1.03070 \cdot \dot{m}_{w,ms} - 0.00198 \qquad \mathrm{COD} = 0.9560 \qquad (37)$$

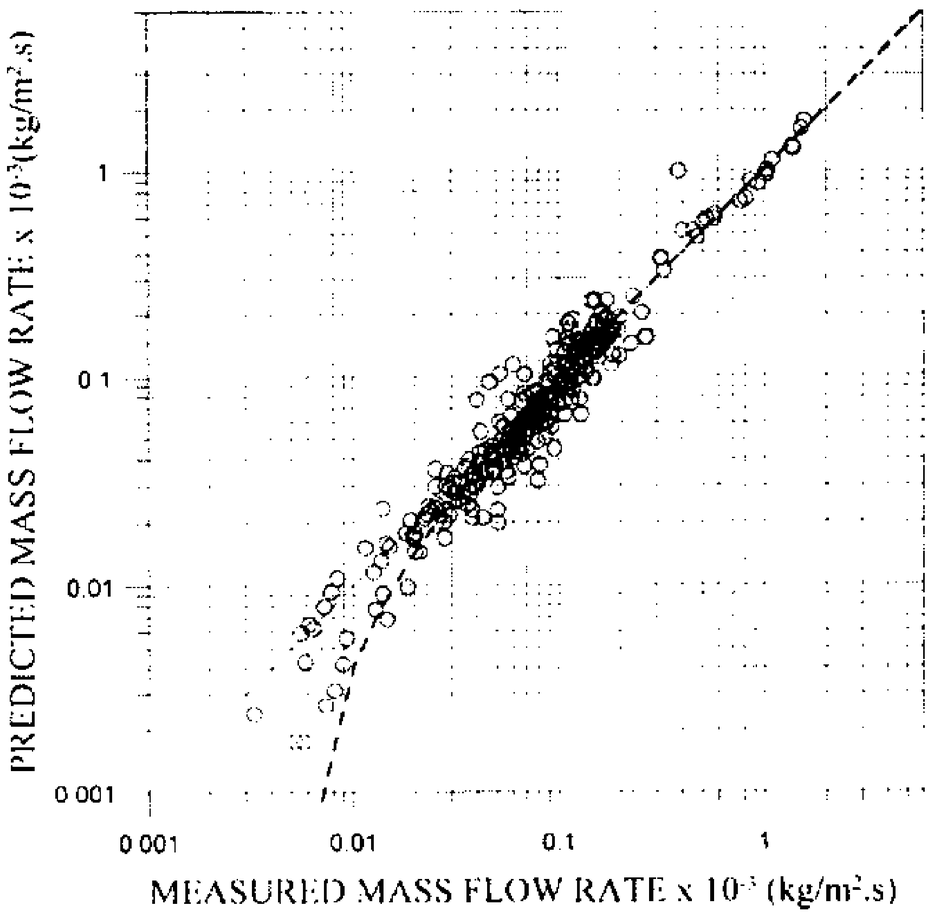

Fig. 12. The yield measurements plotted against predictions according to results from the Chilton–Colburn model and h_{cv} from the refined expression (3) for the complete set of earlier and more recent data.

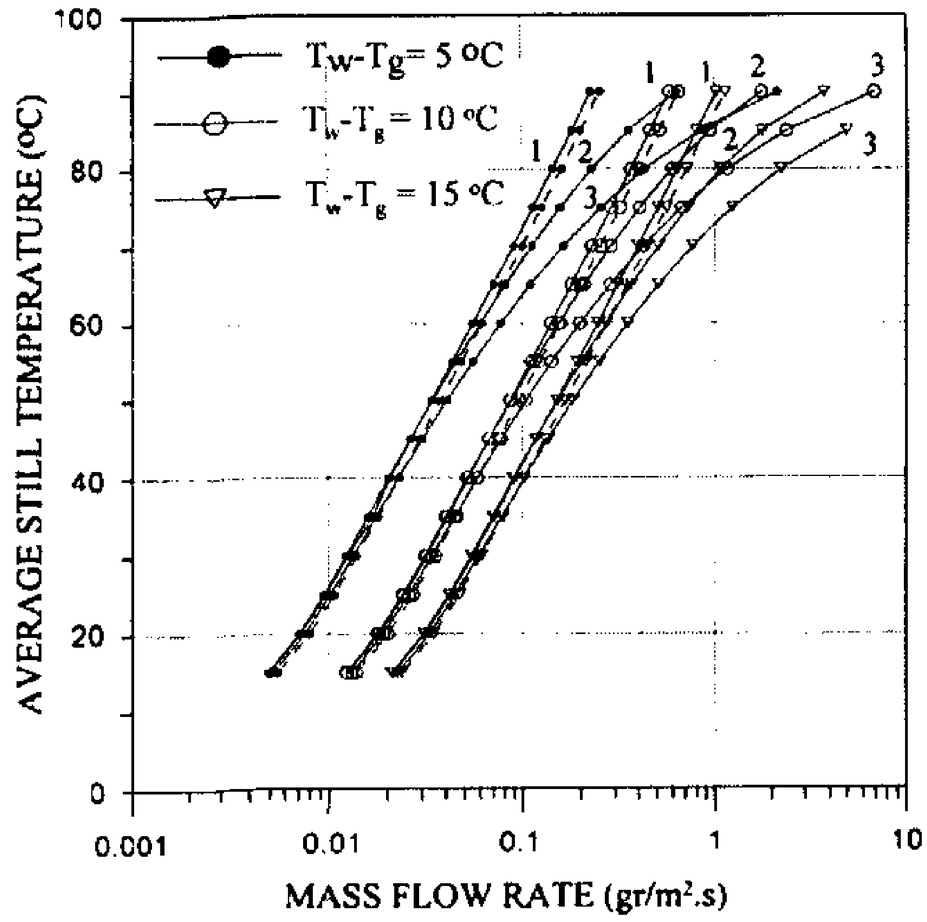

Fig. 13. Comparative presentation of theoretical results according to the basic Dunkle's model (line 1), refined Dunkle's model (line 3) as well as Chilton–Colburn model (line 2), showing the effect of average operating temperature on mass flow rate for $\Delta T = 5$, 10 and 15 °C.

This line which corresponds to an appreciably high coefficient of determination appears to be almost identical to the unity slope line confirming the remarkable accuracy of this model for yield predictions almost over the entire range of measured yields.

7. The influence of average operating temperature of a single effect unit

Among the most crucial quantities affecting the yield is the average operation temperature and the temperature difference between brine and condensing surfaces. Irrespectively of the very high temperature differences that may be developed in the laboratory and although values in excess of 15 °C may not be completely unusual in practice, it can be assumed that depending on specific environmental conditions, ordinary field operation is usually carried out in the range between $5 < \Delta T < 15$ °C as also can be seen in Fig. 1. Aiming to investigate comparably the effect of these two crucial quantities on yield, the predicted mass flow rates were calculated for the whole practical range of $\bar{t}$ and for the fixed values of $\Delta T = 5$, 10 and 15 °C. For each pair of ΔT and $\bar{t}$, the derived temperatures $t_w = \bar{t} + \Delta T/2$ and $t_g = \bar{t} - \Delta T/2$ were employed for the calculation of h_{cv} and $\dot{m}_w$. The results are shown in Fig. 13, in which the average still temperature was plotted against calculated mass flow rates for the three fixed temperature differences of $\Delta T = 5$, 10 and 15 °C corresponding to the three groups of solid lines 1, 2 and 3 respective to the three different employed data points. The three different plotted lines 1, 2 and 3 in each fixed temperature difference group correspond to calculated results according to the simplified Dunkle's model, Chilton–Colburn model and refined Dunkle's model respectively, as derived from the corresponding expressions (10) for $\xi = 0.0144$, (18) and (12), with h_{cv} calculated from (3). Additional results from the simple Dunkle's model for $\xi = 0.162$ have also been comparably plotted with a broken line in each group, indicating a slight parallel shift of the specific curves towards higher yields. It is shown that irrespectively of $\Delta T = T_w - T_g$, there is a very small difference between results for temperature up to about 50 °C. This average temperature for a typical $\Delta T = 10$ °C corresponds to an yield of about 0.1 gr/m^2 s, which becomes a characteristic value beyond of which growing deviations are developed between models. Predictions from the simple Dunkle's and Chilton–Colburn analogy models are almost identical up to about 60 °C irrespectively of ΔT, while at higher average temperatures the predictions from the refined Dunkle's model are becoming increasingly higher. In Fig. 14 the complete set of yield measurements with the earlier and the more recent data being represented by small circles and cross data points respectively were plotted. These data which have been classified into four temperature difference level subgroups, were plotted with specific data points (circles for the earlier, crosses for the more recent data) of four different growing sizes respectively to a growing ΔT in the ranges of $0 < \Delta T < 5$ °C, $5 < \Delta T < 10$ °C, $10 < \Delta T < 15$ °C and $15 < \Delta T < 20$ °C respectively.

In the same figure, three additional solid line curves corresponding to theoretical predictions according to the simplified Dunkle's model and $\xi = 0.0162$ for the respective three temperature difference values of $\Delta T = 5$, 10 and 15 °C were also plotted. It is demonstrated that at least as far as up to about 60 °C is concerned, there is a good agreement between theoretical predictions and measurements. This is indicated by the distribution of recent mea-

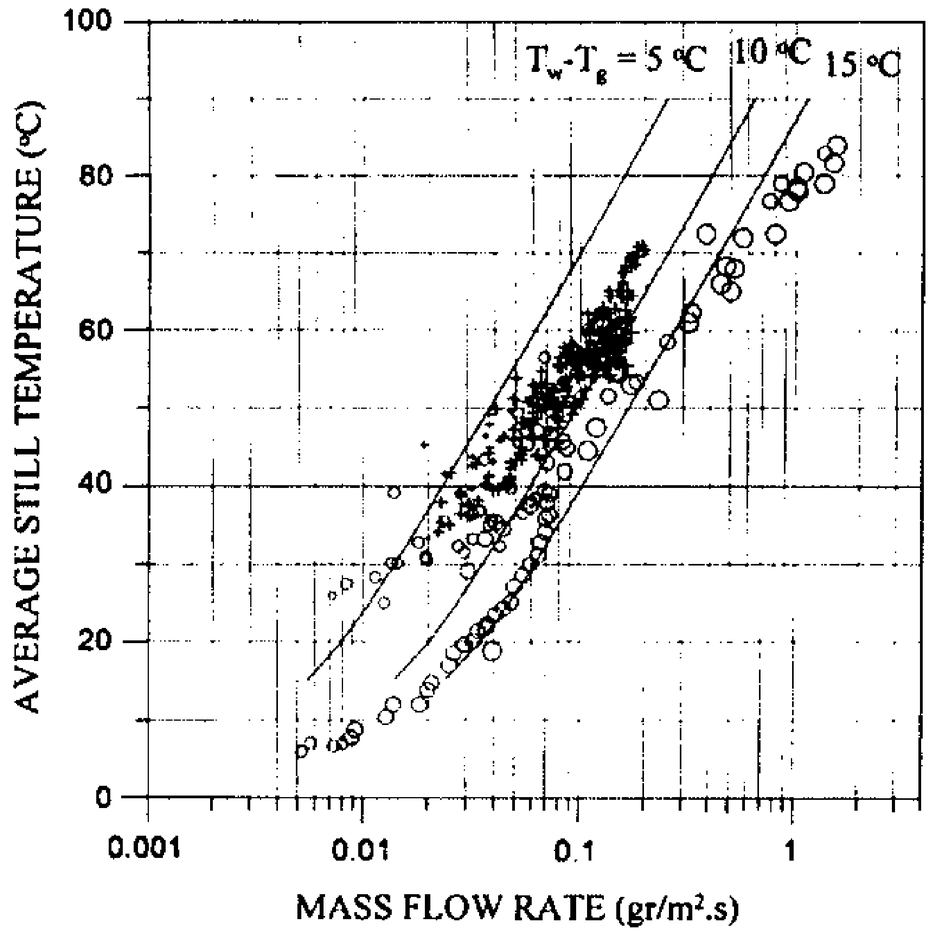

Fig. 14. Comparative presentation of theoretical mass flow rates derived according to basic Dunkle's model and plotted against average temperature through the three solid lines corresponding to $\Delta T = 5$, 10 and 15 °C. In the same plot the complete set of data from earlier and more recent measurements were also drawn using discrete circle and cross data points of four growing sizes corresponding to the respective temperature difference ranges of $0 < \Delta T < 5$ °C, $5 < \Delta T < 10$ °C, $10 < \Delta T < 15$ °C and $\Delta T > 15$ °C.

surements, the majority of which is properly spread close to the $\Delta T = 10$ °C line up to about $\bar{t} = 60$ °C. It is also shown that up to this temperature the respective data points from earlier measurements corresponding to about $12 < \Delta T < 15$ °C, are distributed close to the solid line of $\Delta T = 15$ °C, although at higher $\bar{t}$ they are spread beyond the $\Delta T = 15$ °C theoretical line, indicating a significant underprediction of measurements.

In Fig. 15 the same data are comparably plotted to the three solid lines corresponding to theoretical predictions for $\Delta T = 5$, 10 and 15 °C according to the refined Dunkle's model. It is shown that although there is a good agreement between results at least as far as up to about $\bar{t} = 60$ °C is concerned, at higher $\bar{t}$ and ΔT around 15 °C the data are spread over a region of lower yields than those predicted by the theoretical line $\Delta T = 15$ °C owing to the shift of solid line curves at higher yield values. The same occurs for the recently reported field measurements at higher than about 55 °C, which are now lying closely to the $\Delta T = 5$ instead of $\Delta T = 10$ °C curve, something which indicates overprediction of measurements by this model at higher operating temperatures.

Similar comparative results based on Chilton–Colburn model are shown in Fig. 16. Obviously there is a fairly good agreement between theoretical predictions and measurements at the entire range of average still temperatures up to 85 °C, as it is shown by both, the earlier and the recently reported field measurements, which are appropriately distributed closely to the $\Delta T = 15$ °C and at slightly lower yields relative to the $\Delta T = 10$ °C curve respectively.

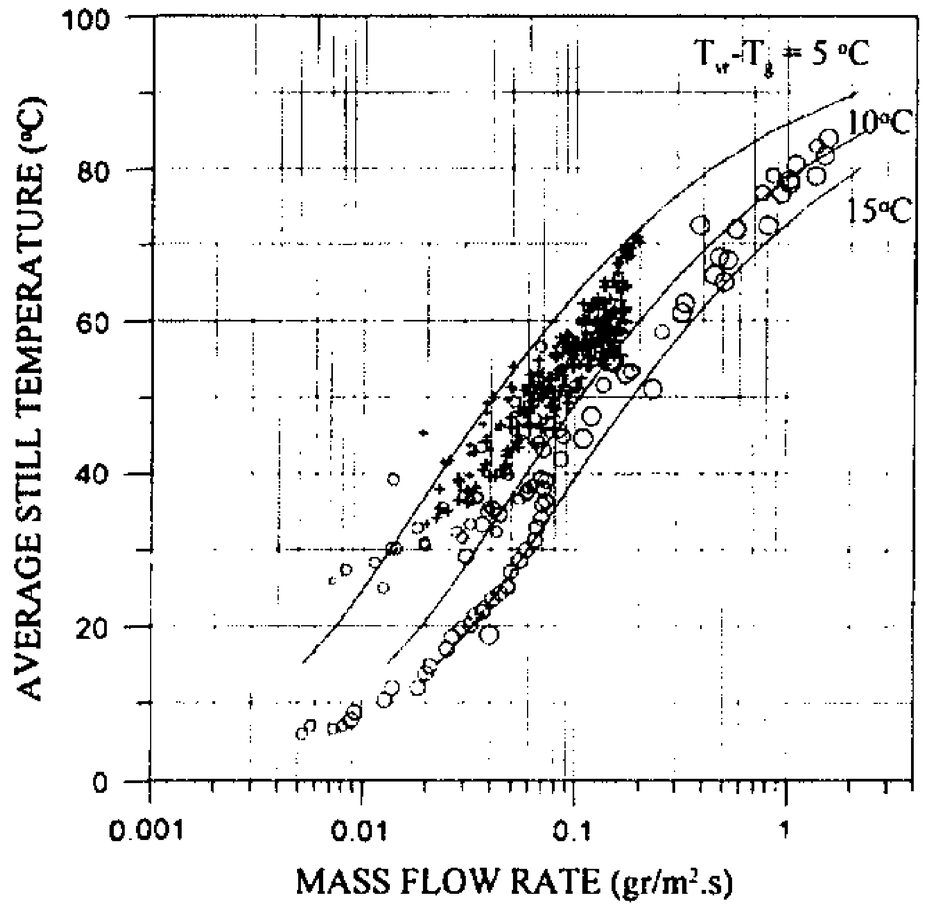

Fig. 15. Comparative presentation of theoretical mass flow rates derived according to the refined Dunkle;s model and plotted against average temperature through the three solid lines corresponding to $\Delta T = 5$, 10 and 15 °C. In the same plot the complete set of data from earlier and more recent measurements were also drawn using discrete circle and cross data points of four growing sizes corresponding to the respective temperature difference ranges of $0 < \Delta T < 5$ °C, $5 < \Delta T < 10$ °C, $10 < \Delta T < 15$ °C and $\Delta T > 15$ °C.

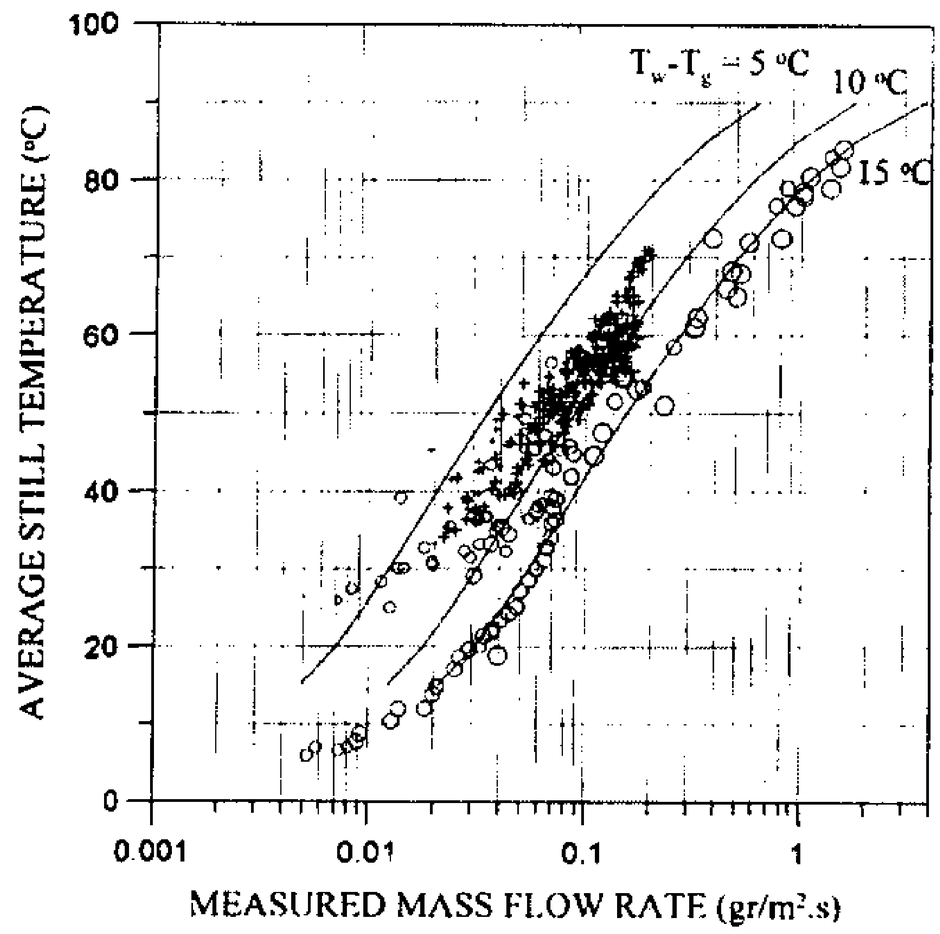

Fig. 16. Comparative presentation of theoretical mass flow rates derived according to the Chilton–Colburn model and plotted against average temperature through the three solid lines corresponding to $\Delta T = 5$, 10 and 15 °C. In the same plot the complete set of data from earlier and more recent measurements were also drawn using discrete circle and cross data points of four growing sizes corresponding to the respective temperature difference ranges of $0 < \Delta T < 5$ °C, $5 < \Delta T < 10$ °C, $10 < \Delta T < 15$ °C and $\Delta T > 15$ °C.

8. Conclusions

The aim of the present work was the investigation of the accuracy level and the validity range of the broadly established theory originally developed by Dunkle, as compared to recently reported mass transfer analyses based on analogy considerations for the prediction the heat and mass transfer processes in solar distillation systems. The validation was based on a massive body of published field and laboratory measurements, covering a wide range of operating conditions. It was derived that the simple model originally developed by Dunkle for ordinary slightly inclined top surface enclosures and appreciably large Raleigh numbers is fairly accurate for yields in excess of the characteristic upper value of 0.1 gr/m^2 s, and anyway lower than about 0.3 gr/m^2 s. This yield corresponding up to about $\bar{t} = 60$ °C °C for $\Delta T = 15$ °C, defines the typical upper limit within a range of yield and average operating temperatures which mostly covers conditions occurring during the practical operation of ordinary solar distillation systems. However at higher yields and operating temperatures it leads to an appreciable underprediction of measurements. It was also derived that the application of the previous model with the original simplifying assumptions relaxed, leads to a substantial overprediction of measurements for higher than about 0.2 gr/m^2 s yields and 55 °C, something which is attributed to the poor modeling of mass transfer phenomena. This contributes to the development of significant prediction errors which are growing as the average temperature rises up to the upper practical maximum operational temperatures.

At the same time, the proposed Chilton–Colburn mass transfer approach appears to model more precisely the mass transfer processes at a broad range of ordinary and very high, at least up to about 2 gr/m^2 s, yields, even employing the simplified convective heat transfer coefficient model which has been originally developed by Dunkle. However, the application of the same mass transfer model taking into consideration the proper temperature dependent saturated mixture properties in the improved accuracy convective heat transfer coefficient expression, leads to an even more precise mass transfer calculation and to an impressively accurate prediction of measurements at a very broad range of yields. This, as far as the available database of measurements is concerned, ranges at least from less than 0.01 up to more than about 2 gr/m^2 s yields, corresponding to temperatures ranging between very low up to almost boiling point values, covering practically the entire possible range of operational temperatures and yields. Although further high temperature validation is pending, the results from the present investigation indicate that the Chilton–Colburn mass transfer model appears to be more accurate and universal in nature, being generally applicable to any cavity design and enclosure geometry for which an accurate specific convective heat transfer correlation will be available.

References

Adhikari, R.S., Kumar, A., Kumar, A., 1990. Estimation of mass-transfer rates in solar stills. Int. J. Energy Res. 14, 737–744.

Aggrawal, S., Tiwari, G.N., 1998. Convective mass transfer in a double – condensing chamber and a conventional solar still. Desalination 115, 181–188.

Clark, J.A., 1990. The steady state performance of a solar still. Solar Energy 44, 43–49.

Corcione, M., 2003. Effects of thermal boundary conditions at the sidewalls upon natural convection in rectangular enclosures heated from below and cooled from above. Int. J. Therm. Sci. 42, 199–208.

Djebedjian, B., Rayan, M.A., 2000. Theoretical investigation on the performance prediction of solar still. Desalination 128, 139–145.

Dunkle, R.V., 1961. Solar Water Distillation: The Roof TypeStill and a Multiple Effect Diffusion Still. In: ASME Proc. Int. Heat Transfer Conf. Part V, Int. Develop. Heat Transfer, Univ. of Colorado, Boulder Colo.

Hollands, K.G.T., Raithby, G.T., Konicek, L., 1975. Correlation equations for free convection heat transfer in horizontal layers of air and water. Int. J. Heat Mass Transfer 18, 879–884.

Hollands, K.G.T., 1984. Multi prandtl number correlation equations for natural convection in layers and enclosures. Int. J. Heat Mass Transfer 27 (3), 466–468.

Hongfei, Zheng, Xiaoyan, Zhang, Jing, Zhang, Yuyuan, Wu, 2002. Group of improved heat and mass transfer correlations in solar stills. Energy Convers. Manage. 43, 2469–2478.

Jakob, M., 1949, first ed.. In: Heat Transfer, vol. 1 Wiley, NY.

Kumar, S., Tiwari, G.N., 1996. Estimation of convective mass transfer in solar distillation systems. Solar Energy 57 (6), 459–464.

Malik, M.A.S., Tiwari, G.N., Kumar, A., Sodha, M.S., 1982. Solar Distillation. Pergamon Press, Oxford, NY.

McAdams, W.H., 1958. Heat Transmission, third ed. Mc Graw-Hill.

Papanicolaou, E., Belessiotis, V., 2005. Double-diffusive natural convection in an asymmetric trapezoidal enclosure: unsteady behavior in the laminar and the turbulent-flow regime. Int. J. Heat Mass Transfer 48, 191–209.

Porta-Gandara, M.A., Rubio-Cerda, E., Fernandez-Zayas, J.L., 1998. Visualization of natural convection inside shallow solar stills. Exp. Fluids 25, 369–370.

Porta-Gandara, M.A., Cervantes, J.G., Solorio, F.J., 2004. Periodic enclosed natural convection in a laboratory solar still. Exp. Fluids 37, 483–487.

Shawaqfeh, Ahmad Taleb, Farid, Mohhamed Mehdi, 1995. New development in the theory of heat and mass transfer in solar stills. Solar Energy 55 (6), 527–535.

Tiwari, G.N., Khan, M.E., Goyal, R.K., 1998. Experimental study of evaporation in distillation. Desalination 115, 121–128.

Tiwari, G.N., Minoha, A., Sharma, P.B., Emran Khan, M., 1997. Simulation of convective mass transfer in a solar distillation process. Energy Convers. Manage. 38 (8), 761–770.

Tsilingiris, P.T., 2007. The influence of binary mixture thermophysical properties in the analysis of heat and mass transfer processes in solar distillation systems. Solar Energy 81, 1482–1491.

Tsilingiris, P.T., 2008. Thermophysical and transport properties of humid air at temperature range between 0 and 100 °C. Energy Convers. & Manage. 49, 1098–1110.

Tsilingiris, P.T., 2009. Analysis of the Heat and Mass Transfer Processes in solar stills – The Validation of a Model. Solar Energy 83, 420–431.

Tsilingiris, P.T., 2010. Modelling heat and mass transport phenomena at higher temperatures in solar distillation systems – the Chilton–Colburn analogy. Solar Energy 84, 308–317.

Tsilingiris, P.T., 2011. Prediction and measurements of mass transport in experimental solar stills. Solar Energy 85, 2561–2570.

Voropoulos, K., Mathioulakis, E., Belesiotis, V., 2000. Transport phenomena and dynamic modeling in greenhouse type solar stills. Desalination 129, 273–281.